SAMPE Quarterly, **23**(2), 29-36 (1992)

Compression Failure Mechanisms of Single-Ply, Unidirectional, Carbon-Fiber Composites

Jong-Bae Ha and John A Nairn
Department of Materials Science and Engineering, University of Utah, Salt Lake City
Received on 9/23/91; revised manuscript received on 1/16/92

ABSTRACT

A single-ply composite compression test was used to study compression failure mechanisms as a function of fiber type, matrix type, and interfacial strength. Composites made with low- and intermediate-modulus fibers (Hercules AS4 and IM7) in either an epoxy (Hercules 3501-6) or a thermoplastic (ULTEM and LARC-TPI) matrix failed by kink banding and out-of-plane slip. The failures proceeded by rapid and catastrophic damage propagation across the specimen width. Composites made with high-modulus fibers (Hercules HMS4/3501-6) had a much lower compression strength. Their failures were characterized by kink banding and longitudinal splitting. The damage propagated slowly across the specimen width. Composites made with fibers treated to give low interfacial strength had low compression strength. These composites typically failed near the specimen ends and had long kink bands.

INTRODUCTION

Because compression fracture of composites often takes place instantaneously, it is difficult to identify the basic compression failure mechanisms of composites. In addition, the presence of defects and misalignment of fibers can bring about completely different failure mechanisms [1]. Therefore, at the present, there is no universally accepted failure mechanism for composites under compression.

Many researchers have studied compression failure mechanisms of composite structures. Among the failure modes that have been proposed are the following: microbuckling of fibers [2-10], kink banding [8,11-20], matrix yielding [21,22], rule of mixtures [23-25], and shear through both the fibers and the matrix [26]. The two analytical approaches most frequently studied are microbuckling of fibers embedded in a polymeric matrix and kink banding. The microbuckling model was first proposed by Rosen [2]. This model over predicts experimental compressive strengths by a factor of two to three. Other researchers [27-29] suggested a variety of schemes to modify Rosen's model to give a more accurate prediction of composite compressive strength.

Several investigators [11,12,19] have addressed kink band formation due to microbuckling. The schematic kink band shown in Figure 1 can be characterized by three parameters: the kink band orientation angle, α, the kink band angle, β, and the kink band length, δ. Berg and Salama [11] were the first to observe kink banding caused by microbuckling of fibers in a carbon fiber/epoxy

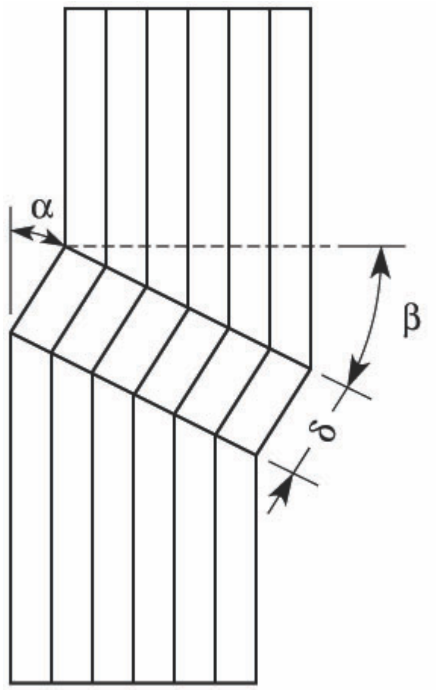

Figure 1: A schematic drawing of a kink band in a composite that fails under compression. The three parameters characterizing the kink band are the kink band orientation angle, α, the kink band angle, β, and the kink band length, δ.

system under axial compression. The orientation of kink bands results from a minimization of strain energy within the bands [12,13,15]. Weaver and Williams [12] have suggested that kink banding is initiated by the transverse fracture of buckled fibers and proceeds by successive buckling and fracture in adjacent fibers. In this manner the kink band broadens and propagates across the composite section. Using notched samples, Chaplin [13] showed that the inclination of the shear band is constant throughout the process. Furthermore, once established from a notch or pre-existing defect, the kink band width is also constant. By considering, both longitudinal, compressive displacement and shear deformation, Chaplin [13] noted that the condition $\alpha=2\beta$ corresponds to a kink band zone whose volume remains constant. A more detailed treatment of the kink banding process is presented by Evans and Adler [15] using a thermodynamic analysis. They derived the relation $\alpha=2\beta$ by minimizing the strain energy in the kink band zone. They also found a value for the preferred kink band orientation by minimizing the plastic work done on the matrix during fiber rotation. By assuming inextensible deformation of the composite under compression, Budiansky [18] predicted the kink band angle for long-wave and short-wave imperfections. He obtained the kink band length by assuming that the matrix is perfectly plastic and that the fibers break when a critical tensile strain is reached at the points of maximum curvature under combined compression and bending. Similarly, Hahn [19,20] determined the three kink band parameters in one unified analysis. He assumed that the matrix is perfectly plastic and that kink band formation is a result of the in-phase bending failure of fibers. He suggested that fiber microbuckling causes kink banding in carbon fiber/epoxy resin, carbon fiber/thermoplastic resin, and glass/epoxy resin composites, but that in Kevlar® aramid fiber/epoxy composites, fiber failure by kinking [30] provokes kink banding of the composite.

Although most investigators treat compression failures in terms of either microbuckling or kink banding, Ewins *et. al.* [31,32] noted compressive failures that were controlled by compression failure of the fibers themselves. They compared axial compression failures of unidirectional laminates to transverse compression failures of laterally constrained, unidirectional laminates. The similarity of the compression strengths and of the fracture morphologies implied that the two types of specimens failed by the same mechanism. Because neither fiber microbuckling nor kink banding is possible in the transverse specimens, Ewins *et. al.* [31,32] concluded that both laminates were controlled by fiber failure. By varying test temperature, Ewins *et. al.* [31,32] observed some failures that included microbuckling and some failures that were dominated by fiber fracture.

In the present study, single-ply, unidirectional composites were tested using a new single-ply composite compression test procedure. Composites were made with three different fiber types (Hercules AS4, IM7, and HMS4) in three different matrices (Hercules 3501-6 epoxy and two thermoplastics — ULTEM and LARC-TPI). To study the effect of the fiber interface, composites were made with sized fibers, unsized fibers, and fibers treated with a release agent. The release agent significantly reduced interfacial strength. An important advantage of the single-ply composite compression test is that because many specimens can be cut from one single-ply composite, it minimizes material requirements. By getting many specimens from each composite, we minimized specimen variability and increased the likelihood of observing basic failure modes as opposed to failure modes influenced by variations in specimen processing.

MATERIALS AND EXPERIMENTAL TEST METHOD

The material systems used in this study include six carbon fiber/epoxy resin composites (AS4/3501-6, AS4G/3501-6, IM7/3501-6, IM7G/3501-6, HMS4/3501-6, HMS4G/3501-6, AS4F/3501-6, IM7F/3501-6, HMS4F/3501-6) and three carbon fiber/thermoplastic resin composites (sized AS4/ULTEM, unsized AS4/ULTEM, AS4/LARC-TPI-PAA+dopant). The Hercules AS4, IM7, and HMS4 fibers were unsized. The Hercules AS4G, IM7G, and HMS4G fibers were coated with an epoxy compatible "G" sizing. The Hercules AS4F, IM7F, and HMS4F were treated with a release agent, Frekote 700. This coating significantly reduced the fiber/matrix interfacial strength. All 3501-6 resin matrix composite samples were provided as β-staged prepreg tapes by Hercules. The prepreg was cured in an autoclave according to manufacturer's recommendations. The composites with thermoplastic matrices (ULTEM and LARC-TPI) were supplied by NASA Langley Research Center as single-ply composites.

To test single-ply composites in compression, we embedded mini-dog-bone specimens in about 20 mils of epoxy and uniaxially end loaded them while supported from the sides by guide blocks [33,34]. End loading was done through shim stock with a thickness that matched each specimen's thickness. The sides of the guide blocks were coated with release agent to minimize friction effects. The dog-bone geometry and the test fixture are shown in Figure 2. The composite compression strength was calculated from the failure load, P_{total}, by a simple rule of mixtures formula

$$\sigma_c = \frac{P_{total} E_c}{E_c A_c + E_e A_e} \tag{1}$$

where E_c and E_e are the moduli of the single-ply composite and of the embedding epoxy. A_c and A_e are the cross-sectional areas of the single-ply composite and of the embedding epoxy at the location of compression failure. E_c and E_e were measured by compression tests on straight-sided single-ply composites. With the mini-dog-bone specimens, the compression failure was almost always at the point of minimum composite cross-sectional area. The compression strengths in this paper were results that were averaged from 15 to 20 nominally identical specimens.

The mini-dog-bone specimen geometry was used to reduce end effects. Compression tests on rectangular, single-ply composites always failed by end crushing [34]. The embedding epoxy was provided additional side support and used to eliminate specimen buckling. Samples that were not embedded failed at low loads by global specimen buckling. By varying the thickness of the

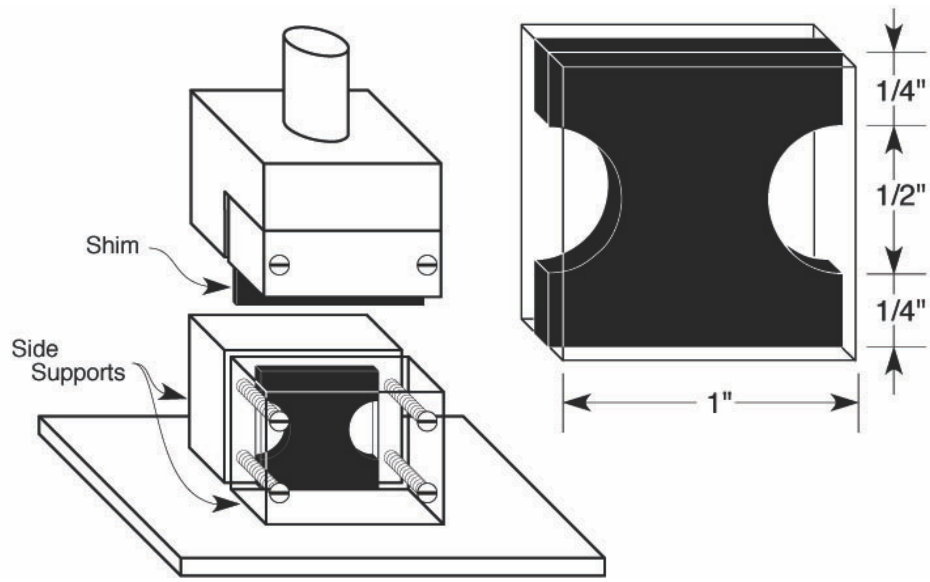

Figure 2: The single-ply composite compression test fixture and an enlargement of the embedded single-ply composite test specimen. The embedded single-ply composite specimens were positioned between two side supports. The rear side support was steel. A transparent, poly-methyl methacrylate front side support was used to permit observation of the failure process. Compression load was applied by a steel shim having a thickness matching that of the embedded single-ply composite specimen.

embedding epoxy we found that σ_c calculated by Eq. (1) increases up to about 20 mils and then becomes constant [34]. We concluded that when the embedding epoxy is too thin, the specimens failed by global buckling, but when the embedding epoxy is sufficiently thick, the specimens failed by axial compressive failure of the single-ply composite. These conclusions are supported by observations of failure modes [34]. Any relatively stiff embedding epoxy can function to prevent buckling. The specimens in this paper used Dow Chemical D.E.R. 332. This epoxy was cured with curing agent, Jeffamine D-230, and with Accelerator 399. Jeffamine D-230 and Accelerator 399 were purchased from Texaco Chemical Co..

Specimen alignment is critical to minimizing experimental scatter. First, the samples must be centered in the embedding epoxy. This centering was achieved by the following procedure: The embedded, single-ply composite specimens were made by curing the embedding epoxy in a mold under pressure in a Carver Hot press. We waited until some initial cure had taken place before applying the pressure. If the pressure was applied too soon after the start of cure, the embedding epoxy viscosity was low and the pressure caused movement of the embedded single-ply composite resulting in poor centering. By waiting before applying pressure, however, the small amount of cure that takes places gave a higher viscosity embedding epoxy. With the higher viscosity embedding epoxy, there was much less movement of the embedded single-ply composite and specimens with good centering alignment could be obtained. Second, the top and bottom of the mini-dog-bone specimen must be parallel. This was achieved by clamping the specimens in a steel jig and sanding their edges flush with the parallel edges of the jig.

We observed compression failure modes by two methods. First, the front, side-support block was made of transparent poly-methyl methacrylate (see Figure 2). We thus observed compression failures as they occurred. Second, following each single-ply composite compression test, the failed specimen was potted in the same embedding epoxy system (D.E.R. 332+D-230+AC 399) to preserve the state of the fracture damage. These potted specimens were cut are various locations and polished with 1 mm and 0.3 mm Al_2O_3 paste on a velvet cloth. The polished specimens were examined by optical microscopy.

EXPERIMENTAL OBSERVATIONS AND RESULTS

The experimental material systems were classified according to four variables. The first variable was fiber type for the same matrix system, such as AS4/3501-6, AS4G/3501-6, IM7/3501-6, IM7G/3501-6, HMS4/3501-6, and HMS4G/3501-6. The second variable was matrix type for the same fiber such as AS4/3501-6, AS4/ULTEM, and AS4/LARC-TPI. The third variable was the presence or absence of applied fiber sizing, such as AS4/3501-6 and AS4G/3501-6 or sized AS4/3501-6 and unsized AS4/3501-6. The fourth variable was the presence or absence of release agent, Frekote 700, such as AS4/3501-6 and AS4F/3501-6. Table 1 lists the compression strengths of all single-ply composites tested. Table 1 also lists the critical fiber fragment lengths that resulted from a single-fiber fragmentation tests on single fibers embedded in an epoxy matrix [35,36]. Qualitatively speaking, the interfacial shear strength for a given fiber is inversely proportional to the critical fiber fragment length [35]. The samples showing infinite critical length resulted from single-fiber fragmentation tests in which the fiber could not be fragmented during tensile loading. These materials have essentially zero interfacial strength.

For composites with the same matrix, but with different fibers, the low- and intermediate-modulus fibers, AS4 and IM7, gave high compression strengths of about 1.4 GPa. These

Material System	Compression Strength (GPa)	Critical Length (mm)	V_f (%)
AS4/3501-6	1.48	0.313	62
IM7/3501-6	1.37	0.332	62
HMS4/3501-6	0.73	0.709	62
AS4G/3501-6	1.47	0.358	62
IM7G/3501-6	1.38	0.332	62
HMS4G/3501-6	0.75	—	62
AS4F/3501-6	0.643	∞	62
IM7F/3501-6	0.629	∞	62
HMS4F/3501-6	0.695	∞	62
AS4/ULTEM sized	1.18	—	61
AS4/ULTEM unsized	1.09	—	56
AS4/LARC-TPI	1.24	—	—

Table 1: The single-ply composite compression strengths and critical length results for various composite materials. The critical length results were measured by a single fiber fragmentation test [35]. A critical length of ∞ means that the fiber was not fragmented during the test and that the interfacial strength is effectively zero.

compression strengths are similar to the compression strengths of multiply AS4/3501-6 laminates [37,38]. The similarity supports our claim that the single-ply composite compression test measures a true in-plane compression strength. The high modulus fiber, HMS4, had a much lower compression strength of about 0.74 GPa. The lower result for HMS4 composites may be due to the fiber being weaker in compression or to other effects unrelated to fiber strength. Some results discussed below suggest that the low compression strength of HMS4 composites was a consequence of the poor fiber/matrix interface in those composites.

The matrix also influenced compression strength. The most complete results were for AS4 fibers in 3501-6 epoxy, ULTEM, or LARC-TPI matrices. The epoxy matrix had the highest compression strength of 1.48 GPa. The two LARC-TPI and ULTEM thermoplastic matrices had lower compression strengths of 1.24 GPa and 1.18 GPa, respectively. In agreement with Rosen's buckling model [2], the compression strengths rank in order of decreasing matrix modulus. The moduli for 3501-6, LARC-TPI, and ULTEM are 3.8 GPa, 3.5 GPa, and 3.0 GPa, respectively [39]

The presence or absence of fiber sizing had little or no effect on composite compression strength. No sizing effect was observed for AS4, IM7, and HMS4 fibers in an 3501-6 epoxy matrix where the fibers were coated or not coated with an epoxy compatible "G" sizing. A small effect was seen for sized and unsized AS4 fibers in an ULTEM matrix. The sized AS4/ULTEM had a compression strength of 1.18 GPa as compared to 1.09 GPa for unsized AS4/ULTEM composites. The sized AS4/ULTEM composites, however, had a higher volume fraction than the unsized AS4/ULTEM composites. The differences in compression strength may be due to the different fiber volume fractions and not to the fiber sizing.

The presence of release agent Frekote 700 had a dramatic effect on compression strength. The AS4F/3501-6, IM7F/3501-6 and HMS4F/3501-6 composites all had compression strengths lower the 0.70 GPa. These were the lowest compression strengths of all samples tested.

To study the effect of interface on composite compression strength we plotted the compression strength as a function of the reciprocal of the critical length. As discussed above the critical length is inversely proportional to the interfacial strength and thus a plot *vs.* the reciprocal of the critical

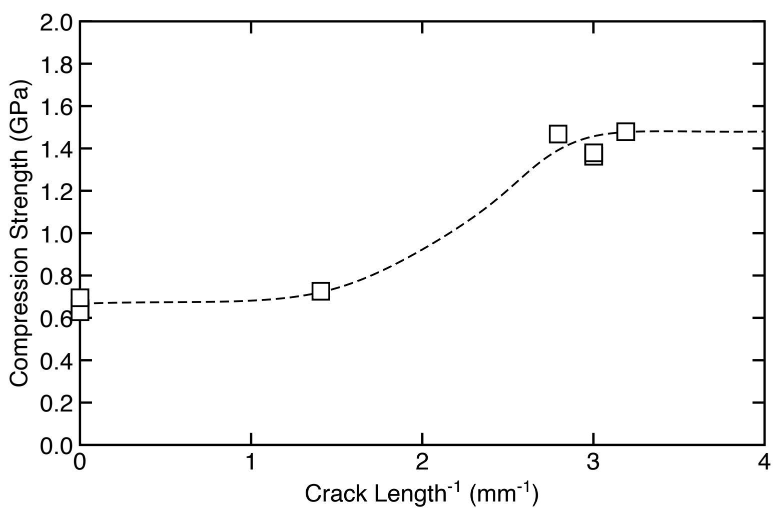

Figure 3: Single-ply composite compression strength as a function of the reciprocal of the critical length. The reciprocal of the critical length is proportional to the interfacial strength.

length is a plot proportional to the interfacial strength. Such a plot in Figure 3 suggests a correlation between composite compression strength and interfacial strength. At low interfacial strength the composite compression strength was also low. All samples having the fibers coated with the release agent (AS4F, IM7F, and HMS4F) had essentially zero interfacial strength ($l_c = \infty$) and a composite compression strength below 0.70 GPa. The HMS4 and HMS4G composites had a better, albeit still poor, interface and compression strengths of 0.74 GPa that were only marginally better than the composites with zero interfacial strength. The AS4 and IM7 composites had the highest interfacial strength and the highest composite compression strength. One conclusion supported by these results is that there is some minimum critical interfacial strength. If the interfacial strength is below the critical minimum, then the composite compression strength will be some low and relatively constant value. If the interfacial strength is high, the compression strength can also be high. The absolute value of the high compression strength will depend on the matrix type and probably on the fiber type. The compression strength cannot increase indefinitely with increases in interfacial strength and thus the curve we sketch in Figure 3 levels off at high interfacial strength. The specific plateau compression strength sketched in Figure 3 assumes it to be similar to the highest compression strengths. This choice was not based on tests with composites having higher compression strengths. If we accept the above conclusions, we can further conclude that the poor compression properties of HMS4 composites were due to a poor fiber/matrix interface and not to an inherent weakness of HMS4 fibers in compression.

An advantage of the single-ply composite compression test is that we can observe compression failure take place. Most specimens fractured at or near the center of the dog-bone shaped specimen. Some fractures occurred suddenly and without warning while others occurred slowly and could be observed to propagate across the width of the specimen. In all cases we stopped the tests as soon as possible after observing failures and then further examined the failed specimens with optical microscopy. Both the quality and the genuineness of the fractured structure depends on how promptly the test is halted after observing the fracture. In some cases, is was not possible to stop the test fast enough to be unambiguously able to describe the failure process.

Compression failures of AS4/3501-6, IM7/3501-6, and AS4/LARC-TPI specimens were characterized by instantaneous and catastrophic failure accompanied by an audible acoustic event. This type of failure was universally observed for defect-free specimens; that is, for well prepared and machined specimens. Typical fractures for these materials are shown in Figure 4. These fractures can all be described by the same failure mechanisms. The failures occurred by kink banding followed by longitudinal propagation of the compression damage parallel to the fibers and by out-of-plane slip along the kink band line. Longitudinal damage propagation results in multiple kink bands in the damage zone (see Figure 4a). Out-of-plane slip along the kink band line is clearly shown in Figure 4c. Because the test could not be stopped soon enough after failure, it was often not possible to capture the details of kink bands or the structure of the longitudinally propagated damage. We suggest that the catastrophic nature of the failure caused some or all of the fractured fibers in the kink bands to be removed during polishing of the specimens.

Because of the high compression strength of AS4/3501-6 and IM7/3501-6 composites and because the AS4 and IM7 fibers have low or intermediate modulus, these specimens were able to withstand the most compressive strain before failure. These material systems, therefore, accumulate high levels of strain energy. At failure the rapid release of strain energy results in instantaneous, catastrophic, and audible failure by kink banding and out-of-plane slip. By the microbuckling models, the fibers will be curved prior to failure. The kink band will start at the point of maximum curvature and proceed in a direction determined by the maximum shear force. The out-of-plane slip will also be along the kink band boundary or maximum shear direction. The amount of out-of-plane slip that is observed will be related to the amount of strain energy released at failure.

Although the failure mechanisms of AS4/3501-6, IM7/3501-6, and AS4/LARC-TPI were similar, the amount of longitudinal propagation of damage in these materials was different. The longitudinal damage propagation area depended on the modulus of fiber and on the matrix. The longitudinal damage propagation area in AS4/3501-6 was typically longer than that of IM7/3501-6 (compare Figures 4a to 4b). Likewise, the longitudinal damage propagation area in AS4/3501-6 was typically longer than that of AS4/LARC-TPI (compare Figures 4a to 4c). These differences can be related to the amount of strain energy present at the time of failure. Comparing AS4/3501-6 to IM7/3501-6, both specimens had the same compression strength and thus the lower-modulus AS4/3501-6 composites had higher strain energy at failure. Comparing AS4/3501-6 and AS4/LARC-TPI, both specimens had the same modulus and thus the higher strength AS4/3501-6 composites had higher strain energy at failure. Therefore, the higher the strain energy at failure, the more extensive is the longitudinal damage propagation area. To be more precise about the longitudinal propagation of damage it would be desirable to observe earlier stages of damage. Although the crosshead speed was decreased from 0.001mm/sec to 0.0001mm/sec for AS4/3501-6 and IM7/3501-6, it was not possible to observe the initiation and longitudinal propagation of compression damage. Fortunately, the results from specimens described below were less instantaneous and catastrophic. Such specimens allowed us to better study the early stages of compression damage.

(a)
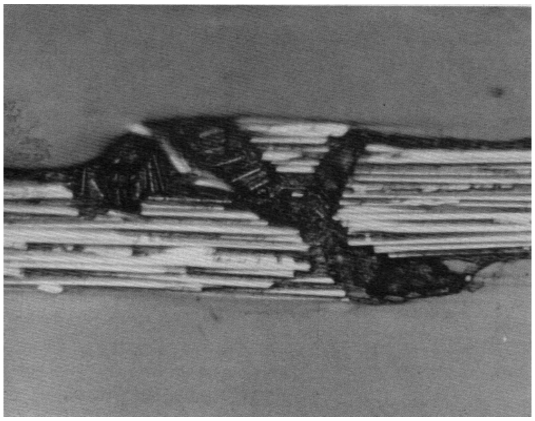

(b)
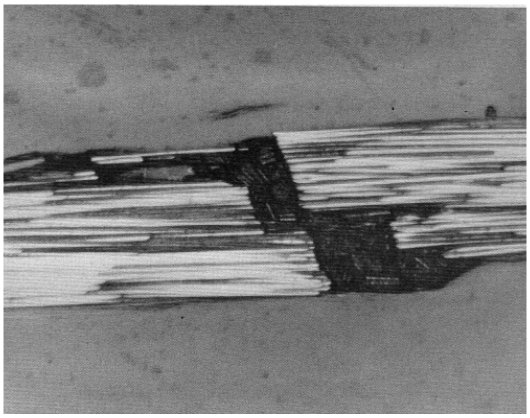

(c)
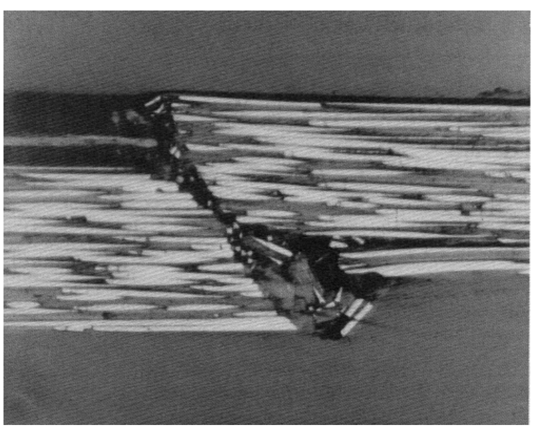

Figure 4: Typical cross sections of compression damage in (a) AS4/3501-6 composites, (b) IM7/3501-6 composites, and (c) AS4/LARC-TPI composites. The crosshead speed was 0.001 mm/sec. The magnification is 200X.

The failure modes of AS4G/3501-6 and IM7G/3501-6 were similar to those of AS4/3501-6 and IM7 3501-6. The "G" sizing on the fiber thus has no effect on the compression strength as well as no effect on the failure modes of these composites.

The fracture phenomenon of sized and unsized AS4/ULTEM composites were characterized by compression damage that rapidly propagated perpendicular to the fiber direction and across the mid-line of the dog-bone. We characterize rapid propagation as damage propagation taking about 0.5 sec to cross the sample width. The rapidly propagating failure of AS4/ULTEM composites is thus less catastrophic than the instantaneous damage observed in AS4/3501-6, IM7/3501-6 and AS4/LARC-TPI composites. The results for AS4/ULTEM composites were not affected by the presence or absence of fiber sizing. Figure 5a. shows a fracture that is typical of both sized AS4/ULTEM and unsized AS4/ULTEM composites. As in AS4/3501-6 composites, the failure occurred by kink banding, out-of-plane slip, and longitudinal propagation of damage. Due to the less catastrophic nature of the failure event and our ability to stop the test sooner, the amount of slip and longitudinal damage propagation is typically less in AS4/ULTEM composites than it is in AS4/3501-6, IM7-3501-6, and AS4/LARC-TPI.

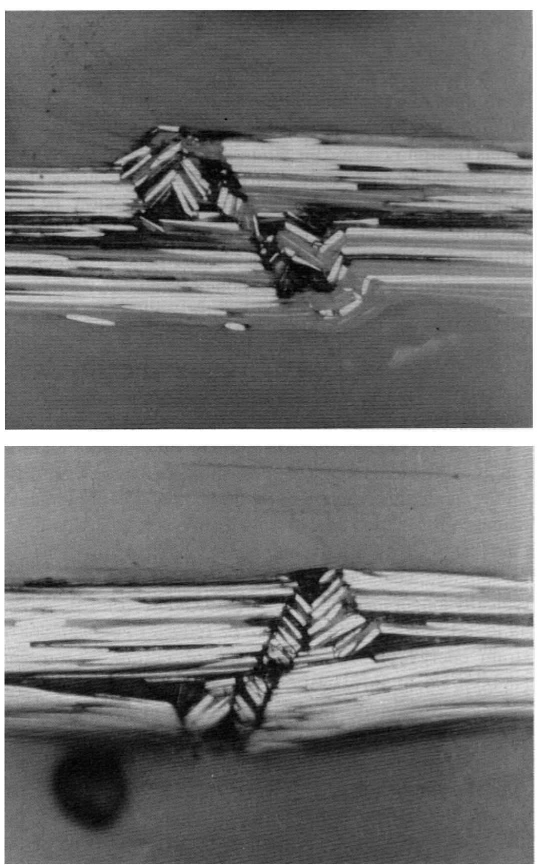

(a)

(b)

Figure 5: Typical cross sections of compression damage in (a) a defect free specimen of sized AS4/ULTEM composites and (b) a sized AS4/ULTEM composite having minor defect. The crosshead speed was 0.001 mm/sec. The magnification is 200X.

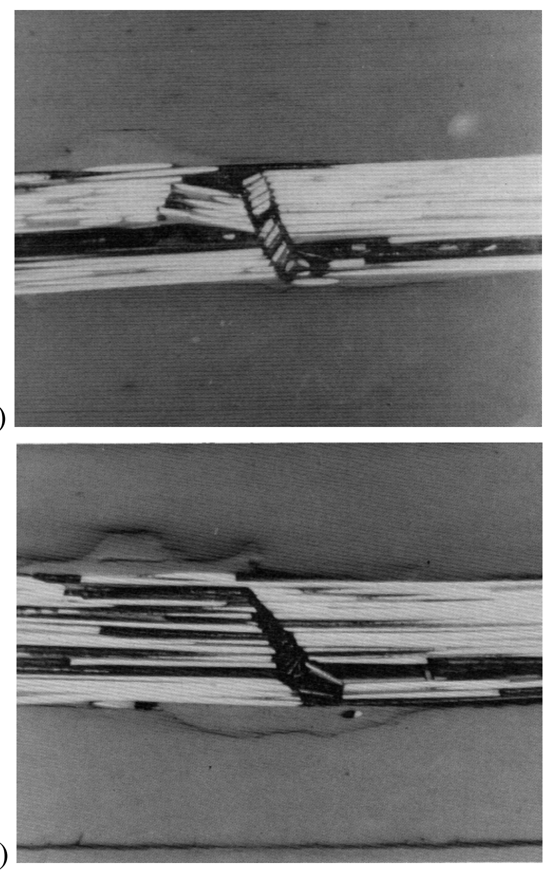

(a)

(b)

Figure 6: Typical cross sections of compression damage in (a) HMS4/3501-6 composites and (b) HMS4/3501-6 composites sectioned near the top of the damage zone. The crosshead speed was 0.001 mm/sec. The magnification is 200X.

Some results from composites that contained pre-existing defects helped us observe the earliest stages of compression damage. In specimens containing pre-existing defects, the damage propagation was less rapid, typically taking 1 to 10 seconds to cross the specimen width. These specimens thus gave us the opportunity to stop the test during the compression failure process. By sectioning near the damage zone tip or just behind it, we observed early forms of compression damage. A typical result for an AS4/ULTEM composites having defects is in Figure 5b. It shows a clear kink band and a longitudinal split. The kink band is just beginning longitudinal propagation into a second kink band. Because less damage has occurred, the fibers remain in the kink band during the polishing process. From these specimens alone we cannot say whether the kink band or the longitudinal split was the first form of damage or whether they occur simultaneously.

Like the defective AS4/ULTEM specimens, defect-free HMS4/3501-6 and HMS4G/3501-6 failed by slow damage propagation typically taking 2 to 10 seconds to cross the specimen width. Figure 6a shows a typical compression damage zone. There is a clear kink band with intact fibers, some longitudinal splitting, and evidence of the initiation of longitudinal propagation of kink banding damage. There is little or no out-of-plane slip along the kink band. We associate the lower amount of out-of-plane slip with the much smaller amount of strain energy released and with our ability to stop the test sooner after failure. The HMS4 laminates failed at a lower load and had a higher modulus. Both of these factors contributed to a much lower sample strain energy at the time of failure.

Figure 6b shows the compression damage at the tip of the compression damage zone from a test that was stopped while the compression damage was propagating across the specimen width. There is a clear longitudinal split and a partial kink band. The implication is that the longitudinal split occurs first and that it initiates the kink band. The kink band then propagates from the longitudinal split and across the thickness of the specimen. Despite careful efforts, however, we were not able to temporally resolve longitudinal split initiation and kink band initiation on the experimental stress-strain curves. It is possible that both failure processes occur simultaneously. We have earlier concluded that the low compression strength of HMS4 composites is due to the poor fiber/matrix interface. It is possible that the poor interface promotes longitudinal splitting. The longitudinal splitting then initiates kink banding and specimen failure.

Figure 7 shows typical fracture features of AS4F/3501-6, IM7F/3501-6, and HMS4F/3501-6 specimens. These specimens had essentially zero interfacial strength and failed by longitudinal splitting initiating at the sample ends. At later stages of damage, the longitudinal splits caused kink bands. The kink band lengths (δ in Figure 1) in composites with zero interfacial strength were always much longer than those of composites with a stronger interface (see Figure 7). The observation of kink bands being caused by longitudinal splits in these composites with zero interfacial strength and the parallel observation of longitudinal splits causing kink bands in HMS4 composites

Figure 7: Typical cross sections of compression damage in composites having the fibers treated with release agent Frekote 700. The crosshead speed was 0.001 mm/sec. The magnification is 200X.

is further evidence that the low compression strength of HMS4 composites is a result of its' poor fiber/matrix interface.

CONCLUSIONS

Individual tests of samples where only the fiber or the matrix change show that both the fiber and the matrix can affect compression strength. The AS4 and IM7 carbon fiber composites have a much higher compression strength than the HMS4 carbon fiber composites. The higher-modulus 3501-6 epoxy matrix composites have a higher compression strength than the two lower-modulus thermoplastic matrix composites.

Because changing the fiber or the matrix also affects the interfacial strength, it is not possible to separate fiber and matrix effects from interfacial strength effects. A plot of all our results as a function of interfacial strength suggests that interfacial strength is crucial to determining the compression strength. More experiments are required to find out under what conditions interfacial strength is important and under what conditions other strength-limiting mechanisms become active.

In composites with low compression strengths, such as HMS4 carbon fiber composites or composites with fibers treated with Frekote 700 release agent, it was possible to observe the earliest stages of compression damage. The results show that longitudinal splitting starts first and that kink bands initiate from the longitudinal splits and propagate across the specimen thickness. At later stages of compression damage the kink banding damage propagates longitudinally resulting in the formation of multiple kink bands. Some samples failed too rapidly to allow observation of the earliest stages of compression damage. Although we have no direct evidence, we hypothesize that these samples also initiate compression failure by longitudinal splitting followed by kink banding. It is possible, however, that samples with high interfacial strength will not show longitudinal splitting. The first form of damage is such specimens would instead be kink banding.

Acknowledgement

This work was supported in part by a contract from NASA Langley Research Center (NAS1-18883) monitored by Dr. Jeff Hinckley.

REFERENCES

1. Hahn, H. T. and Williams, J. G., "Compression Failure Mechanisms in Unidirectional Composites," in *Composites Materials: Testing and Design (7th Conference)*, **ASTM STP 893**, 115 (1986).
2. Rosen, B. W., "Mechanics of Composite Strengthening," in *Fiber Composite Materials*, 58 (American Society of Metals, 1964).
3. Schuerch, H, "Prediction of Compressive Strength in Uniaxial Boron Fiber-Metal Matrix Composite Materials," *AIAA J.*, **4**, 102 (1966).
4. Chung, W. Y. and Testa, R. B., "The Elastic Stability of Fibers in a Composite Plate," *J. Comp. Mat.*, **3**, 58, (1969).
5. Greszczuk, L. B., "Microbuckling Failure of Circular Fiber-Reinforced Composites," *AIAA J.*, **13**, 1311 (1975).
6. Davis, J. G., "Compression Strength of Fiber Reinforced Composite Materials," in *Composite Reliability*, **ASTM STP 580**, 264 (1975).

7. Wang, A. S. D., "A Non-Linear Microbuckling Model Predicting the Compressive Strength of Unidirectional Composites," ASTM paper 78-WA/Aero-1 (1978).
8. Hahn, H. T. and Williams, J. G., "Compression Failure Mechanisms in Unidirectional Composites," NASA TM 85834 (1984).
9. Hahn, H. T., and Sohi, M. M., "Buckling of a fiber Bundle Embedded in Epoxy," *Comp. Sci & Tech.*, **27**, 25 (1986).
10. Purslow, D., "Fractography of Fibre-Reinforced Thermoplastics, Part 3. Tensile, Compressive and Flexural Failure," *Composites*, **19**, 358 (1988).
11. Berg, C. A. and Salama, M., "Fatigue of Graphite Fiber-Reinforced Epoxy in Compression," *Fibre Sci. & Tech.*, **6**, 79 (1973).
12. Weaver, C. W. and Williams, J. G., "Deformation of a Carbon/Epoxy Composite Under Hydrostatic Pressure," *J. Mat. Sci.*, **10**, 1323 (1975).
13. Chaplin, C. R., "Compressive Fracture in Unidirectional Glass-Reinforced Plastics," J. Mat. Sci., **12**, 347 (1977,).
14. Kulkarni, S. V., Rice, J. S., and Rosen B. W. "An Investigation of the Compressive Strength of Kevlar® 49/Epoxy Composites," *Composites*, **6**, 217 (1975).
15. Evans, A. G. and Adler, W. F., "Kinking as a mode of Structural Degradation in Carbon Fiber Composites," *Acta Metallurgica*, **26**, 725 (1978,).
16. Parry, T. V. and Wronski, A. S., "Kinking and Compressive Failure in Uniaxially Aligned Carbon Fiber Composites Tested Under Superposed Hydrostatic Pressure." *J. Mat. Sci.*, **17**, 893 (1982).
17. Wronski, A. S. and Parry, T. V., "Compressive Failure and Kinking in Uniaxially Aligned Glass/Resin Composites Under Superposed Hydrostatic Pressure," J. Mat. Sci., **17**, 3656 (1982).
18. Budiansky, B., "Micromechanics," *Computers and Structures*, **16**, 3 (1983).
19. Hahn, H. T., Sohi, M., and Moon, S., "Compression Failure Mechanisms of Composite Structures," NASA CR 3988 (1986).
20. Hahn, H. T., "Analysis of Kink Band Formation under Compression," *Proceedings of 6th ICCM and 2nd ECCM*, **1** (1987)
21. Swift, D. G., "Elastic Moduli of Fibrous Composites Containing Misaligned Fibers," *J. Physics D: Applied Physics*, **8**, 223 (1975).
22. Piggott, M. R., "A Theoretical Framework for the Compressive Properties of Aligned Fiber Composites," *J. Mat. Sci.*, **16**, 2837 (1981).
23. DeFerran, E. M. and Harris, B., "Compression strength of polyester Resin Reinforced with Steel Wires," *J. Comp. Mat.*, **4**, 62 (1970).
24. Sinclair, J. H. and Chamis, C. C., "Compressive Behavior of Unidirectional Fibrous Composites," in *Compression Testing of Homogeneous Materials and Composites*, **ASTM STP 808**, 155 (1983).
25. Zelenski, E. S., Kuperman, A. M., Bazhenov, S. L., and Berlin, A. A., "Specific Feature of the Mechanical Behavior of Unidirectionally Reinforced Plastics Under Compression," *Proceeding of 6th ICCM and 2nd ECCM*, **1**, 1288 (1987).
26. Hancox, N. L., "The Compression Strength of Unidirectional Carbon Fiber Reinforced Epoxy Resin," J. Mat. Sci., **10**, 234 (1975).
27. Lager, J. L. and June, R. R.,"Design Analysis, Fabrication and Test of a Boron Composite Beam," J. Comp. Mat., **2**, 178 (1968).
28. Moncunill, E., DeFerran, and Harris, B., "Compression Strength of Polyester Resin Reinforced With Steel Wires," J. Comp. Mat., **4**, 62 (1970).
29. Deteresa, S. J., Porter, R. S., and Farris, R. J., "Experimental Verification of a Microbuckling Model for the Axial Compressive Failure of High Performance Polymer Fibres," J. Mate. Sci., **23**, 1886 (1988).
30. Greenwood, J. H., and Rose, P. G., "Compressive Behavior of Kevlar® 49 Fibers and Composites," J. Mat. Sci., **9**, 1809 (1974).
31. Ewins, P. D., and Ham, A. C., "The Nature of Compressive Failure in Unidirectional Carbon Fibre Reinforced Plastics," AIAA/ASME/SAE 15th Structures, Structural Dynamics and Materials Conf., Las Vegas, NV, April 17-19, 1974.

32. Ewins, P. D., and Potter, R. T., "Some Observations on the Nature of Fibre Reinforced Plastics and the Implications in Structural Design," Phil. Trans. R. Soc. Lond. **A294**, 507 (1980).
33. Ha, J. B., Frank, F., Bascom, W. D., and Nairn, J. A, "Compression Testing of Single-Ply Composites," in preparation.
34. Fox, F. G., "Static Compression Test of Single Ply Composites," B. S. Thesis, Material Science and Engineering, University of Utah, June 1989.
35. Bascom, W. D., and Jensen, R. M., "Stress Transfer in Single Fiber/Resin Tensile Tests," *J. Adhesion*, **19**, 219 (1974).
36. Bascom, W. D., personal communication
37. Bascom, W. D., Nairn, J. A., and Boll, D. J., "Studies of Fiber-Matrix Adhesion on Compression Strength," *Proc. of the 1st NASA Advanced Comp. Tech. Conf.*, Seattle, WA, Oct. 29 to Nov. 1, 1990.
38. Odom, E. M., and Adams, D. F., "Failure Modes of Unidirectional Carbon/Epoxy Composite Compression Specimens," *Composites*, **21**, 289 (1990).
39. Leach, D. C., "Continuous Fibre Reinforced Thermoplastic Matrix Composites," in *Advanced Composites*, 43 (Ed. I. K. Partridge, Elsevier Applied Science, London, 1989).